GDCh

Research Articles

Angewandte
Chemie
International Edition
www.angewandte.org

Carbohydrates

Visualizing Chiral Interactions in Carbohydrates Adsorbed on Au(111) by High-Resolution STM Imaging

Johannes Seibel,* Giulio Fittolani, Hossein Mirhosseini, Xu Wu, Stephan Rauschenbach, Kelvin Anggara,* Peter H. Seeberger, Martina Delbianco, Thomas D. Kühne, Uta Schlickum, and Klaus Kern

Abstract: Carbohydrates are the most abundant organic material on Earth and the structural "material of choice" in many living systems. Nevertheless, design and engineering of synthetic carbohydrate materials presently lag behind that for protein and nucleic acids. Bottom-up engineering of carbohydrate materials demands an atomic-level understanding of their molecular structures and interactions in condensed phases. Here, high-resolution scanning tunneling microscopy (STM) is used to visualize at submolecular resolution the three-dimensional structure of cellulose oligomers assembled on Au(1111) and the interactions that drive their assembly. The STM imaging, supported by ab initio calculations, reveals the orientation of all glycosidic bonds and pyranose rings in the oligomers, as well as details of intermolecular interactions between the oligomers. By comparing the assembly of D- and L-oligomers, these interactions are shown to be enantioselective, capable of driving spontaneous enantioseparation of cellulose chains from its unnatural enantiomer and promoting the formation of engineered carbohydrate assemblies in the condensed phases.

Introduction

Elucidating molecular structures and interactions allows us to understand molecular properties in condensed phases. Access to structural information at the atomic level has been tackled by an arsenal of analytical tools ranging from crystallography, spectroscopy, to microscopy. Among these methods, scanning probe microscopy (SPM) has emerged as a non-destructive imaging method capable of resolving molecular structures at the atomic level, particularly when functionalized tips are used.[1–9] This capability has prompted the widespread use of SPM for the characterization of complex molecules,[5–8,10,11] quantum materials,[12–15] photovoltaic materials,[16,17] and catalytic materials.[18] SPM is thereby an attractive tool to establish structure-properties relationships in natural biomaterials, such as complex polysaccharides.[19–24]

Cellulose is the most abundant renewable biopolymer on Earth with an enormous potential as sustainable materials.[25–27] Cellulose properties are controlled by its complex hierarchical structures[22,24,28–31] that display chirality across different scales.[32] At the nanoscale, cellulose is a linear polymer of D-glucose monosaccharides linked to one another via β1,4 linkages. These polymers assemble into fibrils that join together to form larger micron-scale

[*] J. Seibel, X. Wu, S. Rauschenbach, K. Anggara, U. Schlickum, K. Kern
Max Planck Institute for Solid State Research
70569 Stuttgart (Germany)
E-mail: k.anggara@fkf.mpg.de

G. Fittolani, P. H. Seeberger, M. Delbianco
Max Planck Institute of Colloids and Interfaces
14476 Potsdam (Germany)

H. Mirhosseini, T. D. Kühne
Dynamics of Condensed Matter and Center for Sustainable Systems Design, Chair of Theoretical Chemistry, University of Paderborn
33098 Paderborn (Germany)

S. Rauschenbach
Department of Chemistry, University of Oxford
OX13TA Oxford (UK)

G. Fittolani, P. H. Seeberger
Institute for Chemistry and Biochemistry, Free University Berlin
14195 Berlin (Germany)

T. D. Kühne
Center for Advanced Systems Understanding (CASUS) and Helmholtz Zentrum Dresden-Rossendorf
02826 Görlitz (Germany)

J. Seibel, U. Schlickum
Institute of Applied Physics and Laboratory for Emerging Nanometrology, Technische Universität Braunschweig
38104 Braunschweig (Germany)

K. Kern
Institut de Physique, École Polytechnique Fédérale de Lausanne
1015 Lausanne (Switzerland)

J. Seibel
Current address: Institute of Physical Chemistry, Karlsruhe Institute of Technology (KIT)
76131 Karlsruhe (Germany)
E-mail: johannes.seibel@kit.edu

bundles.[31] Structural characterization of cellulose at the micron scale[22–24] has revealed how fibril morphology and size tune the optical, thermal, and mechanical properties of cellulose materials.[33] In contrast, structural characterization of cellulose at the atomic level is lacking[27] due to the structural heterogeneity of naturally sourced samples and the flexibility of carbohydrate chains, making structural analysis by ensemble averaged techniques difficult.[34] Poor understanding of carbohydrate structures and interactions at the atomic level has prevented the development of the carbohydrate materials field that, to date, lags behind the burgeoning fields of protein[35] and DNA[36] nanomaterials design. This is surprising because carbohydrates are the structural "material of choice" in many living systems and the most abundant organic material on Earth.[19–21]

Single molecule studies of carbohydrate structures became possible by combining the Electrospray Ion Beam Deposition (ESIBD) technique and Scanning Tunneling Microscopy (STM), which gave direct access to the assembly,[37,38] connectivity,[39] conformation,[40] and flexibility[41] of single glycans. So far, imaging of single carbohydrate molecules has relied on simple STM topographic imaging using non-functionalized tips that limit the imaging resolution. The use of functionalized tips in molecular imaging is an attractive solution to improve the imaging resolution, permitting the visualization of single covalent bonds in complex molecules.[1–8] Implementing a functionalized tip in carbohydrate imaging thereby holds significant potential to reveal carbohydrate structures and interactions in greater details and improve our understanding of the diverse properties of carbohydrates.[19,20]

Here, we use high resolution STM imaging to visualize intermolecular interactions between cellulose oligomers. We deposited a cellulose hexasaccharide, as a model system for cellulose,[42] on an Au(111) surface held at room temperature using the ESIBD technique.[43,44] We visualized the three-dimensional structures and interactions of the carbohydrate molecules on surface using an STM tip functionalized with a CO molecule. The CO-tipped imaging resolved the orientation of the glycosidic linkages, the geometry of the pyranose rings, as well as the position of the intra- and intermolecular hydrogen bonds that stabilize the assembly of multiple chains. These chiral interactions steer the self-assembly of the carbohydrate molecules, which strikingly result in the spontaneous enantioseparation of D- and L-oligosaccharides in condensed phases. Our work demonstrates the utility of single molecule imaging in unveiling key intermolecular interactions that give rise to carbohydrate assemblies. This knowledge could lead to a better design of carbohydrate materials[21] as well as a better understanding of how carbohydrate surfaces participate in biological contexts.[19,20]

Results and Discussion

D-cellohexaose (D-glucose hexasaccharide linked by β1,4 linkages) was deposited on Au(111) surface using ESIBD[44] and imaged by STM to reveal the structure and self-assembly of the carbohydrate molecules on surface (Figure 1). The cellohexaose oligomers were observed as extended chains with all the pyranose rings of the glucose subunits oriented parallel to the surface.[40] Two geometries were distinguishable by their STM appearances under a metallic tip (Figure 1a): a "Triplet" geometry, consisting of three repeats of glucose dimer; and a "Doublet" geometry, consisting of two repeats of glucose dimer terminated by a glucose monomer at the extremities. Simulated STM images based on Density Functional Theory (DFT) calculations identify the two observed cellohexaose geometries, "Triplet" and "Doublet", as the two ways a ribbon-like cellohexaose molecule can adsorb flat on a surface (Figure 1a). In each geometry, the glycosidic bonds adopt two different orientations, i.e. either pointing down (d) or up (u) (given as red and blue highlights in Figure 1a respectively). In the Doublet geometry, the glycosidic bonds are oriented "ududu" from the non-reducing end to the reducing end; while in the Triplet geometry, they are oriented "dudud". On the surface, molecules in "Triplet" and "Doublet" geometries were observed in equal abundance, and self-assembled into islands with short-range order (Figure S1).

To promote cellohexaose mobility and assembly, we annealed the surface to ≈100 °C. Upon annealing, the cellohexaose molecules exclusively adopted the "Doublet" state and assembled into molecular islands with long-range order (Figure 1b). The exclusive adoption of the "Doublet" state suggests that this orientation is thermodynamically more stable compared to the "Triplet" state, as supported by DFT calculations that show the "Doublet" state to be more stable than the "Triplet" state (SI section S4). The resulting self-assembled structure featured side-by-side assembly of cellohexaose chains, tilted by +75° with respect to the assembly propagation axis (Figure 1b). Detailed analysis of the side-by-side assembly revealed that two cellohexaose molecules form a dimer that repeats along the assembly propagation axis (red brackets in Figure 1b).

To reveal more structural details on the cellohexaose molecules and their assembly, we performed high-resolution STM imaging with a CO-functionalized tip[4,5,45] (Figure 1b). This technique exploits the enhanced imaging resolution as a result of the complex repulsive interaction of the CO molecule on the tip and the underlying molecular structure.[3,45] In brief, the repulsion between the CO and the adsorbed molecule especially in regions with high charge density, such as covalent bonds, causes the CO to undergo a large frustrated rotation that changes the tunneling current significantly for a small tip motion, thereby leading to sharp contrasts in the obtained images. The CO-tipped STM imaging (see Methods) on cellohexaose assemblies revealed submolecular details of individual cellohexaose chains and their intermolecular interactions (Figure 2).

For each cellohexaose molecule, the CO-tipped imaging revealed the three-dimensional structure of the molecule (Figure 2a and Figure S2). The imaging, aided by computed structures from DFT, uncovered the geometry of every glucose subunit as well as the geometry of every glycosidic bond in the molecule. In the non-annealed sample, the CO-tipped imaging clearly differentiated the "Doublet" and
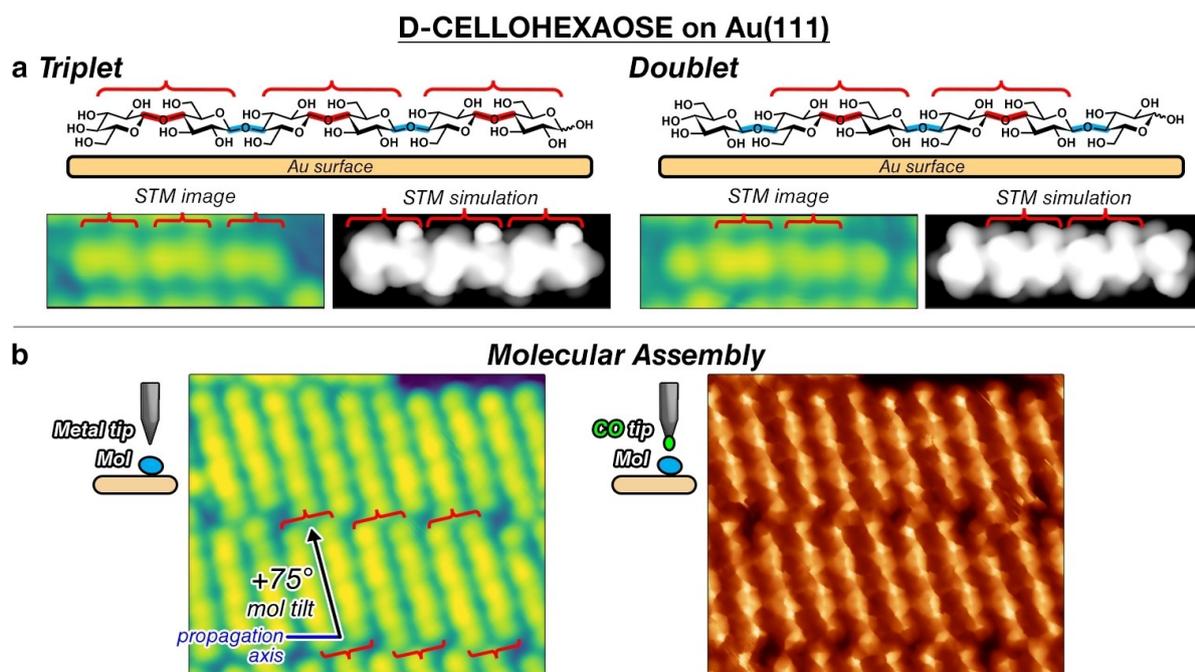
D-CELLOHEXAOSE on Au(111)

Figure 1. STM imaging of cellohexaose on Au(111) surface. (a) D-cellohexaose is a linear D-glucose hexasaccharide linked by β1,4 glycosidic bonds. Cellohexaose was deposited on Au(111) surface and observed by STM as an extended chain that could adopt either of the two different geometries, termed "Triplet" and "Doublet". (b) Cellohexaose molecules self-assembled on surface with a +75° tilt from the assembly propagation axis (defined as the direction to which the assembly grows). The structures were imaged by a CO-functionalized tip to reveal more structural details for every cellohexaose molecule on surface. The molecules were observed to assemble as dimers (marked by repeating red brackets).
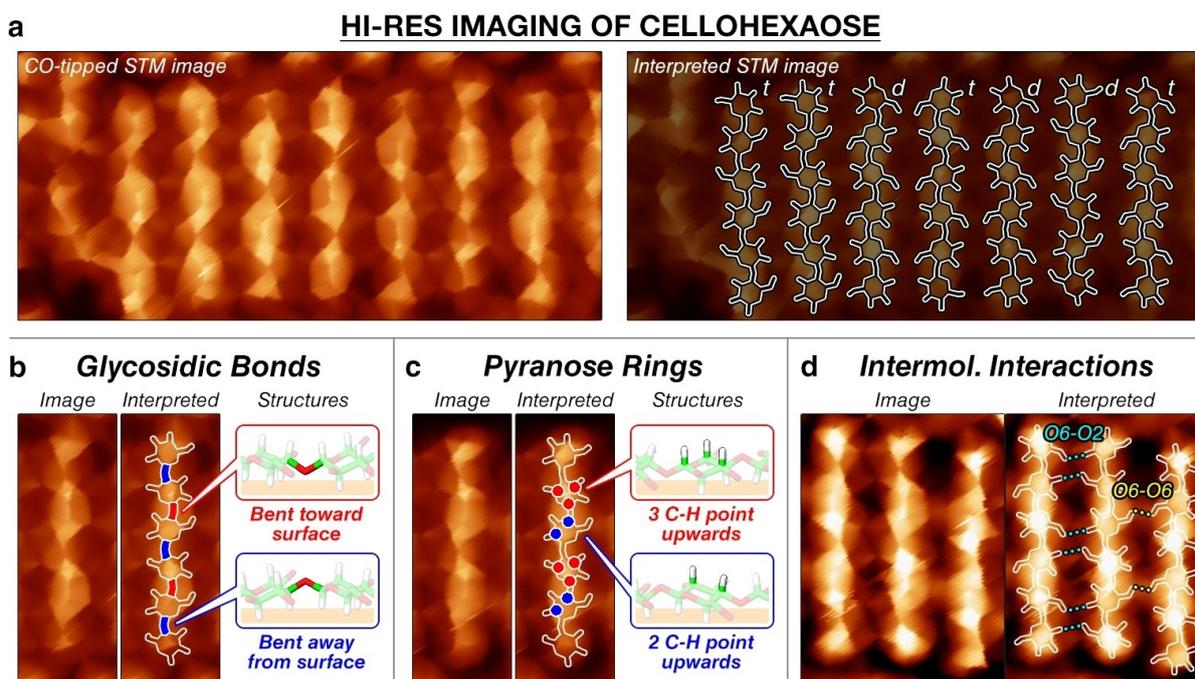
HI-RES IMAGING OF CELLOHEXAOSE

Figure 2. CO-tipped STM imaging of cellohexaose assembly on Au(111) surface. (a) CO-tipped STM images were obtained for non-annealed sample as constant current STM images using a CO-functionalized tip at 6 K. Comparing CO-tipped STM image and DFT optimized structures enables the clear identification of cellohexaose "Doublet" (*d*) and "Triplet" (*t*) structures on surface. CO-tipped imaging permitted the characterization of the glycosidic bonds in Panel (b), pyranose rings in Panel (c), as well as the intermolecular interactions between cellohexaose molecules in the ordered assemblies in Panel (d). We only show cellohexaose in its "Doublet" state in Panel (b–d) because they were the only species found on surface after annealing.

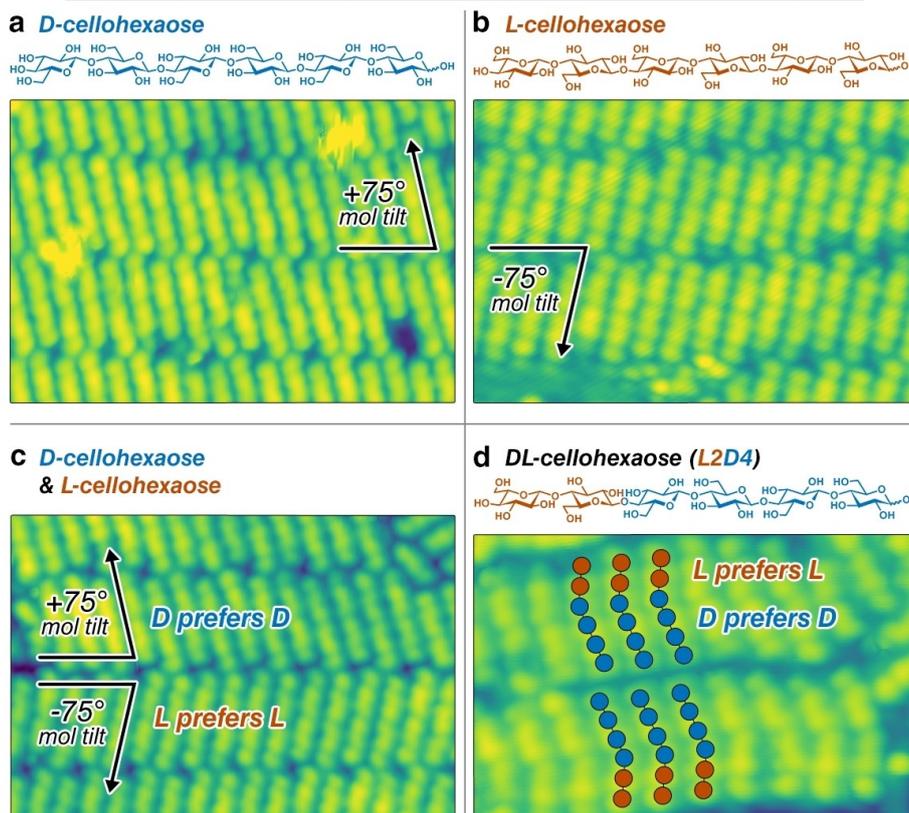**Figure 3.** STM imaging of chiral interactions in cellohexaose assembly on Au(111) surface. Cellohexaose assembles with +75° tilt along the assembly propagation axis for D-cellohexaose in (a), and with −75° tilt for L-cellohexaose in (b). (c) Conglomerate was observed when both D- and L-cellohexaose were present on surface, giving domains that exclusively contain D-cellohexaose and domains that exclusively contain L-cellohexaose due to the preferential D–D and L–L interactions. (d) The preferential D–D and L–L interactions were operative on cellohexaose with mixed chirality, here demonstrated for L2D4.

"Triplet" states of cellohexaose (Figure 2a). By taking a closer look at individual molecules, the CO-tipped imaging located the glycosidic bonds and resolve them as dark and bright lines that correspond to the glycosidic bonds that are closer to the tip (bent away from the surface) or further from the tip (bent toward the surface), respectively (Figure 2b). We understand these contrast to originate from the orientation of C–H bonds neighboring the glycosidic bond, as revealed by our simulations with the Probe Particle Model[3,45] (see Methods): when the glycosidic bond bends toward the surface, the adjacent C–H bonds point up to give the bright contrast; whereas when the glycosidic bond bends away from the surface the C–H bonds point down to give the dark contrast (Figure S2). In addition, the CO-tipped imaging resolved the pyranose rings as bright and dim features, which correspond to the pyranose ring oriented with three C–H bonds pointing upwards towards the tip or with two C–H bonds pointing upwards towards the tip, respectively (Figure 2c). These interpretations are corroborated by simulations using Probe Particle Model[3,45] that shows the C–H bonds pointing upward to be the main contributors of the observed CO-tipped contrast. As a result, three C–H bonds pointing up give a brighter contrast

than two C–H bond pointing up (Figure S2). The more varied appearance for the pyranose rings at the termini of cellohexaose is likely due to their varied tilts on surface.[40] Resolving glycosidic bonds and pyranose rings in a cellohexaose molecule thereby allows for both the reducing and non-reducing ends of the molecule to be inferred. Such information indicates that the cellohexaoses assemble in anti-parallel fashion in the ordered assemblies found after annealing (Figure 2d), consistent with the DFT calculations which describe the anti-parallel cellohexaose dimer as the thermodynamically most stable structure (Table S1).

Interestingly, the CO-tipped imaging gave contrast between "Doublet" cellohexaose molecules, indicating the locations of hydroxyl residues and their role in intermolecular interactions (Figure 2d), as observed previously for other systems.[45] The contrast observed between the cellohexaose molecules in a dimer unit suggests hydrogen bonding interactions between the C6–OH and C2–OH (labeled O6–O2 in Figure 2d), whilst the contrast observed between cellohexaose molecules in neighboring dimer units suggests interactions between their C6–OH residues (labeled O6–O6 in Figure 2d). The latter interactions result in observed offset between adjacent dimers, leading to the 75° tilt angle

between the molecular long axes and their propagation direction (Figure S3). Our findings identify these highly selective hydrogen bonding interactions as one of the important driving forces[31] behind cellohexaose self-assembly on surfaces.

The interactions between cellohexaose molecules unveiled by the CO-tipped imaging provide a clear example of chirality transmission from the molecular (sub-nanometer) scale to the mesoscopic (sub-micron) scale.[46,47] The angle of +75° between the D-cellohexaose axis and the propagation direction of the side-by-side assembly renders the assembly chiral (Figure 1c). To further investigate the role of chirality in the self-assembly process, we deposited and imaged L-cellohexaose on Au(111). L-cellohexaose yielded side-by-side assembly structures that propagates at −75° with respect to the molecular chain axis, perfectly mirroring the self-assembled structures obtained from D-cellohexaose (Figure 3a, 3b).

To examine whether the chiral interactions in cellohexaose chains change when both enantiomers are present on surface, we co-deposited a racemic mixture of D- and L-cellohexaose molecules. Interestingly, the D- and L- cellohexaose molecules formed their respective chiral domains, evidencing conglomerate formation[48] (Figure 3c and Figure S4) similar to the previously observed dipeptide assembly on surface.[49] We confirmed the homochirality of the domains by examining the unit cell parameters of the self-assembled structures, as well as by looking at the CO-tipped imaging (Figure S5). When the two domains were in contact, two types of domain boundaries were observed, formed either by side-by-side or head-to-head interactions (Figure S5). The conglomerate formation is understood to be due to the preferential D-glucose—D-glucose and L-glucose—L-glucose interactions.

The highly selective D-glucose—D-glucose and L-glucose—L-glucose interactions open new possibilities to influence the final mesoscopic self-assembled carbohydrate structures.[50] We demonstrate such a possibility by depositing and imaging a cellohexaose molecule that consists of both D- and L-glucose subunits, L2D4 (Figure 3d). We observed the formation of self-assembled structures comprising of extended chains of cellohexaose interacting side-by-side (Figure 3d). The molecules were observed with a slight offset that separates the oligomer into a group of four and two glucose subunits (Figure 3d), thereby revealing the locations of the D- and L-glucose units in the molecule.

For every L2D4-cellohexaose (Figure 3d), the L-glucose domain of the molecule was observed to preferentially bind to the L-glucose subunits of the neighboring molecules, and likewise for the D-glucose domain of the molecule. The observed structures demonstrate the enantioselective interactions in cellulose assemblies on surface, which could offer new opportunities in the design of carbohydrate materials[21] as well as in understanding carbohydrate interactions in biological systems.[19,20] We further confirmed this observation by using CO-tipped imaging to resolve the three-dimensional structures of L2D4-cellohexaose on surface (Figure S6). By comparing the CO-tipped imaging of L2D4-cellohexaose, D-cellohexaose, and L-cellohexaose, we un-

equivocally identified the D- and L-glucose domains in the molecule, confirming that the preferential D–D and L–L interactions drive the self-assembly of L2D4. This result suggests the potential of CO-tipped imaging for analytical purposes,[51] by identifying every constituent monosaccharide in any carbohydrate molecules that can be deposited on surface.

Conclusion

We report the use of single molecule imaging to reveal intermolecular interactions between carbohydrate oligomers. We show that the CO-tipped STM imaging reveals the three-dimensional structure of carbohydrate molecules on surface, as well as the structural features driving carbohydrate-carbohydrate interactions at the atomic level. Examining the interactions of cellohexaose as a model for cellulose —the most abundant biomolecule on Earth—we discovered enantioselective interactions between D-glucose oligomers. These interactions drive the formation of a D-cellohexaose —L-cellohexaose conglomerate on surface, the first example of crystallization-based separation of carbohydrates on surface due to their chiral recognition. These results demonstrate the tandem combination of ESIBD and single molecule imaging as a valuable tool to characterize carbohydrate molecules and their interactions, expanding our understanding of the rich and complex chemistry of carbohydrates.

Author Contributions

J.S., K.A., M.D., U.S., K.K. conceived the project. J.S. performed the scanning tunneling microscopy measurements. K.A., X.W., and S.R. performed the ESIBD experiments. G.F., M.D., and P.H.S. synthesized the glycan molecules. H.M. and T.D.K. performed the calculations. J.S. and K.A. wrote the paper with input from all authors. All authors contributed to the manuscript.

Acknowledgements

[1] L. Gross, F. Mohn, N. Moll, P. Liljeroth, G. Meyer, *Science* **2009**, *325*, 1110–1114.

[2] L. Gross, *Nat. Chem.* **2011**, *3*, 273–278.

[3] P. Jelínek, *J. Phys. Condens. Matter* **2017**, *29*, 343002.

[4] G. Kichin, C. Weiss, C. Wagner, F. S. Tautz, R. Temirov, *J. Am. Chem. Soc.* **2011**, *133*, 16847–16851.

[5] J. Lawrence, G. C. Sosso, L. Đorđević, H. Pinfold, D. Bonifazi, G. Costantini, *Nat. Commun.* **2020**, *11*, 2103.

[6] D. Ebeling, M. Šekutor, M. Stiefermann, J. Tschakert, J. E. P. Dahl, R. M. K. Carlson, A. Schirmeisen, P. R. Schreiner, *Nat. Commun.* **2018**, *9*, 2420.

[7] R. Pawlak, J. G. Vilhena, A. Hinaut, T. Meier, T. Glatzel, A. Baratoff, E. Gnecco, R. Pérez, E. Meyer, *Nat. Commun.* **2019**, *10*, 685.

[8] A. Hinaut, T. Meier, R. Pawlak, S. Feund, R. Jöhr, S. Kawai, T. Glatzel, S. Decurtins, K. Müllen, A. Narita, S. X. Liu, E. Meyer, *Nanoscale* **2018**, *10*, 1337–1344.

[9] B. Alldritt, P. Hapala, N. Oinonen, F. Urtev, O. Krejci, F. Federici Canova, J. Kannala, F. Schulz, P. Liljeroth, A. S. Foster, *Sci. Adv.* **2020**, *6*, eaay6913.

[10] B. Schuler, G. Meyer, D. Peña, O. C. Mullins, L. Gross, *J. Am. Chem. Soc.* **2015**, *137*, 9870–9876.

[11] K. Kaiser, F. Schulz, J. F. Maillard, F. Hermann, I. Pozo, D. Peña, H. J. Cleaves, A. S. Burton, G. Danger, C. Afonso, S. Sandford, L. Gross, *Meteorit. Planet. Sci.* **2022**, *57*, 644–656.

[12] O. Gröning, S. Wang, X. Yao, C. A. Pignedoli, G. Borin Barin, C. Daniels, A. Cupo, V. Meunier, X. Feng, A. Narita, K. Müllen, P. Ruffieux, R. Fasel, *Nature* **2018**, *560*, 209–213.

[13] D. J. Rizzo, G. Veber, T. Cao, C. Bronner, T. Chen, F. Zhao, H. Rodriguez, S. G. Louie, M. F. Crommie, F. R. Fischer, *Nature* **2018**, *560*, 204–208.

[14] S. Mishra, X. Yao, Q. Chen, K. Eimre, O. Gröning, R. Ortiz, M. Di Giovannantonio, J. C. Sancho-García, J. Fernández-Rossier, C. A. Pignedoli, K. Müllen, P. Ruffieux, A. Narita, R. Fasel, *Nat. Chem.* **2021**, *13*, 581–586.

[15] Y. Zhao, K. Jiang, C. Li, Y. Liu, G. Zhu, M. Pizzochero, E. Kaxiras, D. Guan, Y. Li, H. Zheng, C. Liu, J. Jia, M. Qin, X. Zhuang, S. Wang, *Nat. Chem.* **2023**, *15*, 53–60.

[16] T. Meier, R. Pawlak, S. Kawai, Y. Geng, X. Liu, S. Decurtins, P. Hapala, A. Baratoff, S. X. Liu, P. Jelínek, E. Meyer, T. Glatzel, *ACS Nano* **2017**, *11*, 8413–8420.

[17] D. A. Warr, L. M. A. Perdigão, H. Pinfold, J. Blohm, D. Stringer, A. Leventis, H. Bronstein, A. Troisi, G. Costantini, *Sci. Adv.* **2018**, *4*, eaas9543.

[18] J. V. Lauritsen, M. Reichling, *J. Phys. Condens. Matter* **2010**, *22*, 263001.

[19] A. Varki, *Glycobiology* **2017**, *27*, 3–49.

[20] A. Varki, R. D. Cummings, J. D. Esko, P. Stanley, G. W. Hart, M. Aebi, D. Mohnen, T. Kinoshita, N. H. Packer, J. H. Prestegard, R. L. Schnaar, P. H. Seeberger, *Essentials of Glycobiology*, Cold Spring Harbor Laboratory Press, Cold Spring Harbor **2022**.

[21] M. Delbianco, P. Bharate, S. Varela-Aramburu, P. H. Seeberger, *Chem. Rev.* **2016**, *116*, 1693–1752.

[22] R. R. Lahiji, X. Xu, R. Reifenberger, A. Raman, A. Rudie, R. J. Moon, *Langmuir* **2010**, *26*, 4480–4488.

[23] I. Usov, G. Nyström, J. Adamcik, S. Handschin, C. Schütz, A. Fall, L. Bergström, R. Mezzenga, *Nat. Commun.* **2015**, *6*, 7564.

[24] P. N. Ciesielski, R. Wagner, V. S. Bharadwaj, J. Killgore, A. Mittal, G. T. Beckham, S. R. Decker, M. E. Himmel, M. F. Crowley, *Proc. Natl. Acad. Sci. USA* **2019**, *116*, 9825–9830.

[25] D. Klemm, B. Heublein, H. P. Fink, A. Bohn, *Angew. Chem. Int. Ed.* **2005**, *44*, 3358–3393.

[26] B. Thomas, M. C. Raj, B. K. Athira, H. M. Rubiyah, J. Joy, A. Moores, G. L. Drisko, C. Sanchez, *Chem. Rev.* **2018**, *118*, 11575–11625.

[27] T. Li, C. Chen, A. H. Brozena, J. Y. Zhu, L. Xu, C. Driemeier, J. Dai, O. J. Rojas, A. Isogai, L. Wågberg, L. Hu, *Nature* **2021**, *590*, 47–56.

[28] M. Jarvis, *Nature* **2003**, *426*, 611–612.

[29] A. N. Fernandes, L. H. Thomas, C. M. Altaner, P. Callow, V. T. Forsyth, D. C. Apperley, C. J. Kennedy, M. C. Jarvis, *Proc. Natl. Acad. Sci. USA* **2011**, *108*, E1195–E1203.

[30] H. Zhu, S. Zhu, Z. Jia, S. Parvinian, Y. Li, O. Vaaland, L. Hu, T. Li, *Proc. Natl. Acad. Sci. USA* **2015**, *112*, 8971–8976.

[31] M. Wohlert, T. Benselfelt, L. Wågberg, I. Furó, L. A. Berglund, J. Wohlert, *Cellulose* **2022**, *29*, 1–23.

[32] B. Frka-Petesic, S. Vignolini, *Nat. Photonics* **2019**, *13*, 365–367.

[33] R. M. Parker, G. Guidetti, C. A. Williams, T. Zhao, A. Narkevicius, S. Vignolini, B. R. Frka-Petesic M Parker, G. Guidetti, C. A. Williams, T. Zhao, A. Narkevicius, S. Vignolini, B. Frka-Petesic, *Adv. Mater.* **2018**, *30*, 1704477.

[34] M. R. Wormald, A. J. Petrescu, Y. L. Pao, A. Glithero, T. Elliott, R. A. Dwek, *Chem. Rev.* **2002**, *102*, 371–386.

[35] P. S. Huang, S. E. Boyken, D. Baker, *Nature* **2016**, *537*, 320–327.

[36] S. Dey, C. Fan, K. V. Gothelf, J. Li, C. Lin, L. Liu, N. Liu, M. A. D. Nijenhuis, B. Saccà, F. C. Simmel, H. Yan, P. Zhan, *Nat. Rev. Methods Primers* **2021**, *1*, 13.

[37] S. Abb, N. Tarrat, J. Cortés, B. Andriyevsky, L. Harnau, J. C. Schön, S. Rauschenbach, K. Kern, *Angew. Chem. Int. Ed.* **2019**, *58*, 8336–8340.

[38] S. Abb, N. Tarrat, J. Cortés, B. Andriyevsky, L. Harnau, J. C. Schön, S. Rauschenbach, K. Kern, *RSC Adv.* **2019**, *9*, 35813–35819.

[39] X. Wu, M. Delbianco, K. Anggara, T. Michnowicz, A. Pardo-Vargas, P. Bharate, S. Sen, M. Pristl, S. Rauschenbach, U. Schlickum, S. Abb, P. H. Seeberger, K. Kern, *Nature* **2020**, *582*, 375.

[40] K. Anggara, Y. Zhu, M. Delbianco, S. Rauschenbach, S. Abb, P. H. Seeberger, K. Kern, *J. Am. Chem. Soc.* **2020**, *142*, 21420–21427.

[41] K. Anggara, Y. Zhu, G. Fittolani, Y. Yu, T. Tyrikos-Ergas, M. Delbianco, S. Rauschenbach, S. Abb, P. H. Seeberger, K. Kern, *Proc. Natl. Acad. Sci. USA* **2021**, *118*, e2102168118.

[42] M. Delbianco, A. Kononov, A. Poveda, Y. Yu, T. Diercks, J. Jiménez-Barbero, P. H. Seeberger, *J. Am. Chem. Soc.* **2018**, *140*, 5421–5426.

[43] V. Grill, J. Shen, C. Evans, R. G. Cooks, *Rev. Sci. Instrum.* **2001**, *72*, 3149–3179.

[44] S. Rauschenbach, M. Ternes, L. Harnau, K. Kern, *Annu. Rev. Anal. Chem.* **2016**, *9*, 473–498.

[45] P. Hapala, G. Kichin, C. Wagner, F. S. Tautz, R. Temirov, P. Jelínek, *Phys. Rev. B* **2014**, *90*, 085421.

[46] G. Fittolani, D. Vargová, P. H. Seeberger, Y. Ogawa, M. Delbianco, *J. Am. Chem. Soc.* **2022**, *144*, 12469–12475.

[47] R. Fasel, M. Parschau, K. H. Ernst, *Angew. Chem. Int. Ed.* **2003**, *42*, 5178–5181.

[48] S. Srisanga, J. H. Ter Horst, *Cryst. Growth Des.* **2010**, *10*, 1808–1812.

[49] M. Lingenfelder, G. Tomba, G. Costantini, L. C. Ciacchi, A. De Vita, K. Kern, *Angew. Chem. Int. Ed.* **2007**, *46*, 4492–4495.

[50] S. Gim, G. Fittolani, Y. Nishiyama, P. H. Seeberger, Y. Ogawa, M. Delbianco, *Angew. Chem. Int. Ed.* **2020**, *59*, 22577–22583.

[51] C. J. Gray, L. G. Migas, P. E. Barran, K. Pagel, P. H. Seeberger, C. E. Eyers, G. J. Boons, N. L. B. Pohl, I. Compagnon, G. Widmalm, S. L. Flitsch, *J. Am. Chem. Soc.* **2019**, *141*, 14463–14479.
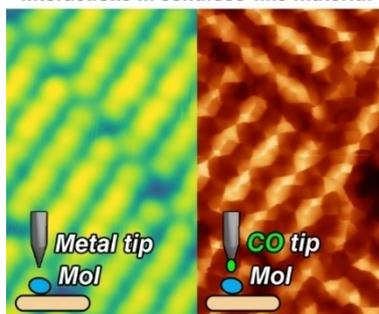
Research Articles

Carbohydrates

J. Seibel,* G. Fittolani, H. Mirhosseini,
X. Wu, S. Rauschenbach, K. Anggara,*
P. H. Seeberger, M. Delbianco, T. D. Kühne,
U. Schlickum, K. Kern ——— e202305733

Visualizing Chiral Interactions in Carbohydrates Adsorbed on Au(111) by High-Resolution STM Imaging

Interactions in cellulose-like material

Metal tip
Mol

CO tip
Mol

Scanning tunneling microscopy is used to visualize molecular structures and interactions in a cellulose oligomer assembly. High-resolution imaging with CO-modified tips, supported by ab initio calculations, reveals the orientation of all glycosidic bonds and pyranose rings in the oligomers and details of intermolecular interactions between the oligomers. Comparing the assembly of *D*- and *L*- oligomers shows their spontaneous enantioseparation.